Available online at www.sciencedirect.com
ScienceDirect
Journal of Power Sources 173 (2007) 877–881
JOURNAL OF POWER SOURCES
www.elsevier.com/locate/jpowsour

Short communication

Ethanol oxidation on hexagonal tungsten carbide single nanocrystal-supported Pd electrocatalyst

Feng Ping Hu, Pei Kang Shen *

State Key Laboratory of Optoelectronic Materials and Technologies, School of Physics and Engineering, Sun Yat-Sen University, Guangzhou 510275, PR China

Received 13 July 2007; received in revised form 12 August 2007; accepted 13 August 2007
Available online 24 August 2007

Abstract

Hexagonal tungsten carbide single nanocrystal has been prepared by the intermittent microwave heating (IMH) technique. The structural information of the nanomaterial is obtained by the TEM, fast Fourier transform (FFT) of the HRTEM, XRD and electrochemical measurements. The hexagonal tungsten carbide single nanocrystal is used as smart support of the Pd-based electrocatalysts (Pd–WC/C) for the oxidation of ethanol in alkaline media. The results show that the 50 wt%Pd–WC/C gives the best performance. The significant improvement in the catalytic activity compared to that of the Pd/C is believed due to the higher electrochemical active surface area (EASA) and the synergistic effect between Pd and WC.

Keywords: Hexagonal tungsten carbide; Intermittent microwave heating; Ethanol oxidation; Electrocatalyst; Fuel cell

1. Introduction

The reduction in the cost of liquid fuel cells is extremely important for practical applications. Attempts have been focused on either exploring non-noble catalysts or reducing the Pt loadings by forming Pt alloys with others metals such as Ru, Fe, Co, Ni, Cu and so on [1,2] to cut the catalyst cost. Among various non-noble catalysts, transition metal oxides [3] or transition chalcogenides [4,5] as Pt alternatives are frequently studied. On the other hand, tungsten carbides or nitrides as novel supports were also intensively investigated to enhance the activity of Pt-based electrocatalysts or to reduce the Pt loadings in the electrocatalysts [6–9]. It has been proved that tungsten carbides are stable in acidic solution as a support of fuel cell electrocatalyst [10]. Tungsten carbide had been used for hydrogenation, dehydrogenation, isomerization in chemical catalysis [11,12] and hydrogen ionization and hydrogenation [13,14] in electrocatalysis owing to its capability to resistant the poisoning of carbon monoxide, hydrocarbons and hydrogen sulfide under high concentration [15]. The catalytic activity of tungsten carbide could be improved by various methods such as the direct carburization of tungsten powder, solid-state metathesis, mechanical milling and polymeric precursor routes using metal alkoxides [16–19]. Recently, various types of tungsten carbides including WC nanorods thin film [20], WC nanotubes [21,22], tungsten carbide microspheres [23], tungsten carbide porous sphere core [24], hollow global tungsten carbide [25] were successfully synthesized and investigated. However, most of the preparation processes of WC need the high temperature and hydrogen or other reductive atmosphere.

We had prepared WC crystal by an intermittent microwave heating (IMH) technique and used as catalyst support for oxygen reduction. IMH is an effective method to rapidly synthesize nanocrystals with controllable particle size in one step process [26–28]. Here, we report the preparation of hexagonal tungsten carbide single nanocrystal and the characterization on the catalytic activity for ethanol oxidation as Pd-based electrocatalyst support.

2. Experimental

Tungsten powder (1 g) was added into 25 mL of aqueous solution containing 10 mL of 30% (v/v) H_2O_2, 5 mL of 2-

* Corresponding author. Tel.: +86 20 84036736; fax: +86 20 84113369.
E-mail address: stsspk@mail.sysu.edu.cn (P.K. Shen).

0378-7753/$ – see front matter © 2007 Elsevier B.V. All rights reserved.
doi:10.1016/j.jpowsour.2007.08.042

propanol, and 10 mL of water. The solution was left to rest for 24 h before Vulcan XC-72 carbon powder (Cabot Corp., USA) was added. The mixture was treated in an ultrasonic bath to form uniformly dispersed ink. The ink was then dried in a microwave oven with a heating procedure of 5 s on and 5 s pause for six times. The dried powder was used as the precursor of tungsten carbides. The precursor powders in the quartz tube were further treated by the intermittent microwave heating procedure after 10 min of argon bubbling. The hexagonal tungsten carbide single nanocrystal was obtained. Pd supported on WC (Pd–WC/C) was prepared and used as electrocatalyst for the oxidation of ethanol. Pd–WC/C and Pd/C electrocatalysts were prepared by the reduction of $PdCl_2$ aqueous solution (4.7 ml, 0.1 mol dm^{-3}) on 50.0 mg carbon or WC. The formic acid (5 ml, 1 mol dm^{-3}) was used as reducing agent. The mixture was put into a microwave oven (1000 W, 2.45 GHz, Galanz, China) and was then alternatively heated for 20 s and paused for 60 s for six times. The Pd loadings on the Pd/C and Pd–WC/C electrodes were both controlled at 0.3 mg cm^{-2} [29].

Chemicals were of analytical grade and used as received. The experiments were carried out at 30 °C controlled by a water-bath thermostat. Structural characterization was conducted on a JOEP JEM-2010 (JEOL Ltd.) transmission electron microscopy (TEM) operating at 200 kV and an X-ray diffractometer (D/Max-IIIA, Rigaku Co., Japan, Cu K_1 (λ = 1.54056 A°) radiation). All electrochemical measurements were performed in a three-electrode cell on an IM6e electrochemical workstation (Zahner-Electrik, Germany). A platinum foil (3.0 cm^2) and Hg/HgO (1.0 mol dm^{-3} KOH) were used as counter and reference electrodes, respectively.

3. Results and discussion

Fig. 1 shows the typical transmission electron microscopic (TEM) images of the tungsten carbide on carbon. The TEM images indicate that the tungsten carbides prepared by the IMH method are nanosized hexagonal particles. The average particle size is about 20 nm according to Fig. 1b. The high-resolution TEM (HRTEM) images (Fig. 1c and d) and the fast Fourier transform algorithm (FFT) image (inset in Fig. 1c) show that the two dimensional structure of hexagonal tungsten carbide nanocrystal is grown along the zone axis [0 0 1], the lattice spacings are $d = 2.556$ Å and $d = 2.586$ Å.

The X-ray diffraction (XRD) measurement (Fig. 2) further confirmed that the tungsten carbides prepared by the present method are nanocrystals. The XRD patterns of the tungsten carbide nanocrystals clearly show the existence of crystalline WC. The 2θ of 31.50, 35.66, 48.36, 64.02, 65.86, 73.14, 75.52 and 77.16 with the d values of 2.8377, 2.5156, 1.8805, 1.4531,

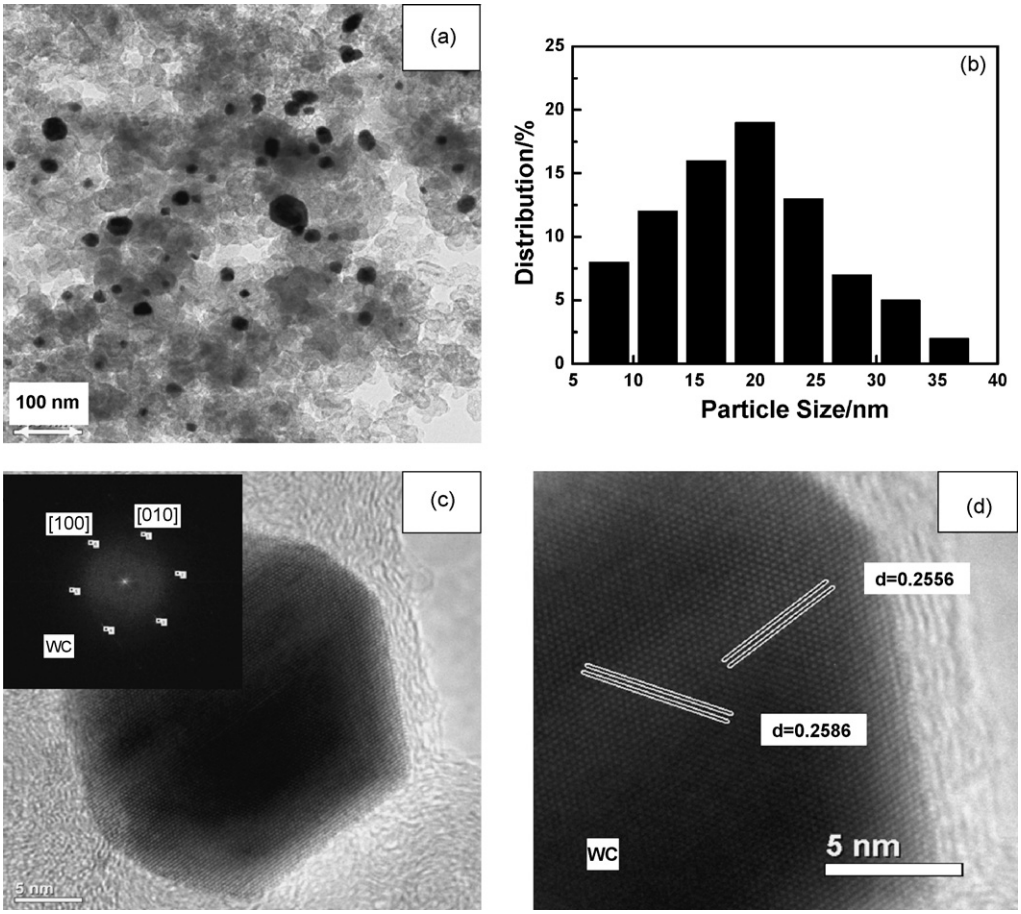

Fig. 1. TEM images of: (a) WC (inset is EDS of WC); (b) the size distribution of WC (data from (a)); (c) HRTEM of WC (inset is the fast Fourier transform algorithm (FFT) image); and (d) the enlarged HRTEM image of WC (c).

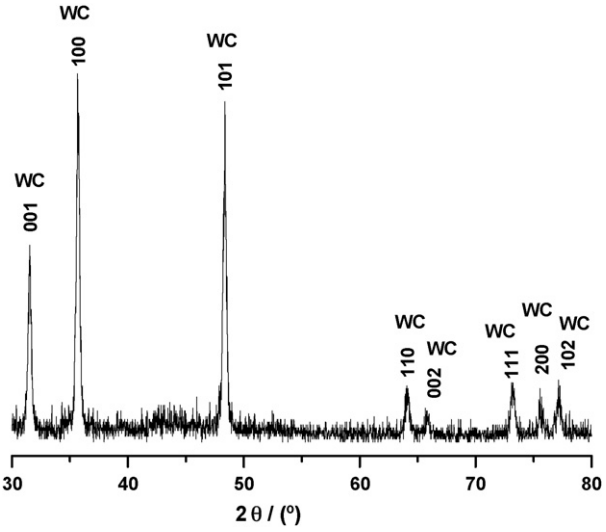

Fig. 2. XRD pattern of WC.

1.4164, 1.2928, 1.2579 and 1.2352 correspond to the (0 0 1), (1 0 0), (1 0 1), (1 1 0), (0 0 2), (1 1 1), (2 0 0) and (1 0 2) facets of WC.

The hexagonal tungsten carbide single nanocrystals were used as support to prepare Pd-based electrocatalysts for ethanol oxidation. As we known, Pd is active for ethanol oxidation in alkaline solution as previously reported [30,31]. Fig. 3a shows the typical cyclic voltammograms of 50 wt%Pd–WC/C for ethanol oxidation in 1.0 mol dm^{-3} KOH/1.0 mol dm^{-3} ethanol solution at room temperature. The curves show the characteristic peaks of ethanol oxidation. The Pd–WC/C electrocatalyst shows a significantly high activity compared to that of Pd/C with the more negative onset potential and higher peak current densities. One interesting feature is that the forward peak potential and backward peak potential are very close for the ethanol oxidation on the novel electrocatalyst. This indicates that the recovering of the activity of the electrode is faster for the 50 wt%Pd–WC/C electrocatalyst than that of Pd/C electrocatalyst. This evidenced that the novel electrocatalyst could sustain higher potential polarization. From the inset of Fig. 3a we can find that the novel electrocatalyst has higher electrochemical active surface area (EASA) which may mainly contribute to the higher catalytic activity.

The *R* shown in Fig. 3b denotes the ratio of the current density of ethanol oxidation on Pd–WC/C to the current density of ethanol oxidation on Pd/C at certain potential. It shows that the *R* values are over 5 at the potentials ranging from −0.55 to −0.2 V. The larger *R* values at lower potentials are favorable for a fuel cell to output larger voltage.

Different Pd loadings on WC/C support electrocatalysts were prepared and were used to fabricate electrodes. The EASA of each electrode was firstly determined by measuring hydrogen adsorption/desorption charges on the cyclic voltammogram in 1.0 mol dm^{-3} KOH solution. The second column in Table 1 compares the EASA in mC cm^{-2}. It is obvious that the 50 wt% Pd–WC/C electrode gives the largest EASA. The data of EASA, onset potential and current densities at different potentials of various electrocatalysts for ethanol oxidation are shown in Table 1.

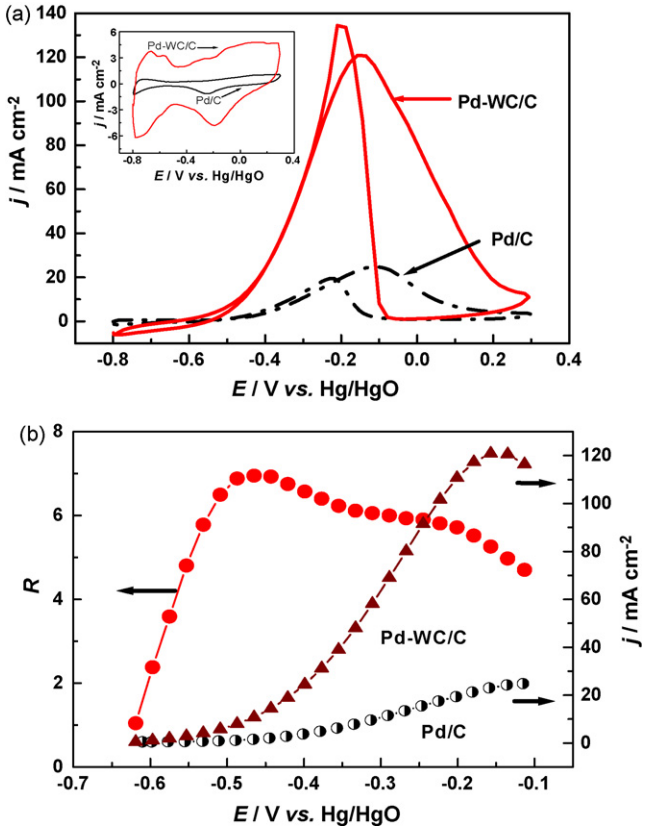

Fig. 3. (a) Cyclic voltammograms of ethanol oxidation on Pd/C and 50 wt% Pd–WC/C in 1.0 mol dm^{-3} KOH/1.0 mol dm^{-3} ethanol solution at 303 K, scan rate: 50 mV s^{-1} (inset is the cyclic voltammograms of Pd/C and 50 wt% Pd–WC/C in 1.0 mol dm^{-3} KOH). (b) Forward potential sweep curves of ethanol oxidation on Pd/C and 50 wt% Pd–WC/C (right) and the ratios *R* (left) between that of Pd–WC/C with Pd/C.

It shows that the higher the EASA, the larger the peak current density and current density at −0.3 V is.

The data of the second column and fourth column in Table 1 were normalized against the corresponding data of Pd/C and re-plotted the data as the ratios of the EASAs and the ratios of peak current densities in Fig. 4. Both the ratios of the EASAs and the ratios of the peak current densities of the different electrodes gave the similar tendency. It shows a volcano relationship between the ratios of the EASAs or the ratios of peak current densities and the percentage of Pd in the electrocatalysts, indicating that two contrary factors may underlie the composition

Table 1
Electrocatalytic activity of various electrocatalysts for ethanol oxidation

Electrocatalysts	EASA (mC cm^{-2})	Onset potential (V)	j_p (mA cm^{-2})	j at −0.3 V (mA cm^{-2})
WC/C	0	0	0	0
10 wt% Pd–WC/C	3.52	−0.599	53.2	26.7
20 wt% Pd–WC/C	5.36	−0.623	66. 4	33.6
40 wt% Pd–WC/C	6.88	−0.619	74. 2	47.4
50 wt% Pd–WC/C	9.34	−0.641	121.1	65.1
60 wt% Pd–WC/C	8.99	−0.649	90. 3	61.1
80 wt% Pd–WC/C	4.61	−0.633	59. 5	28.3
Pd/C	1.92	−0.524	24.82	12.5

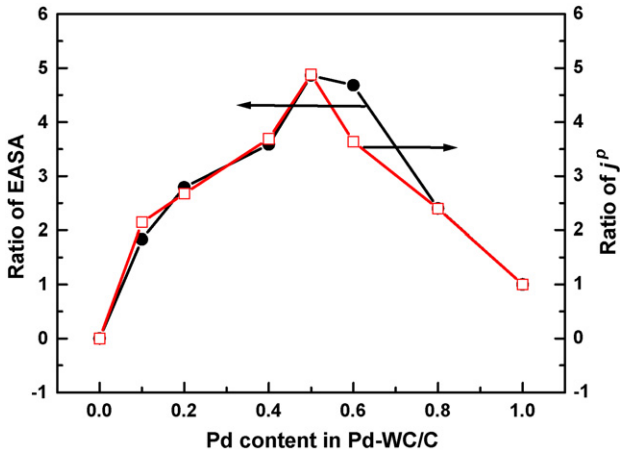

Fig. 4. The relationship between Pd content in electrocatalyst and the ratios of EASAs or peak current densities (j_p) of the different Pd-based electrocatalysts against that of Pd/C.

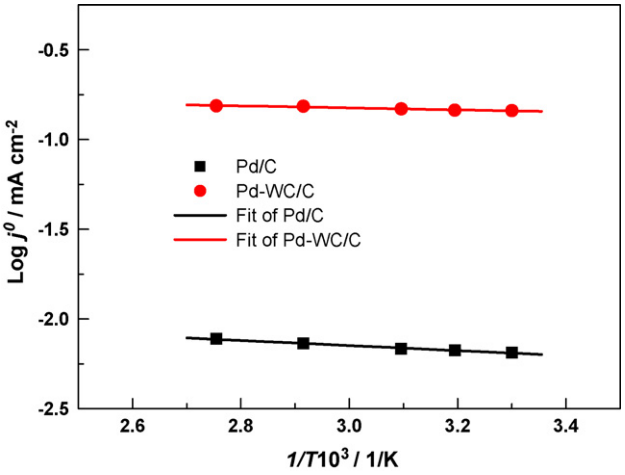

Fig. 5. Log j^0 − 1/T plots of ethanol oxidation on Pd–WC/C and Pd/C at different temperatures of 303 K, 313 K, 323 K, 343 K and 363 K.

effect. At lower Pd percentages, the EASAs and catalytic activities increase with increasing the Pd contents. It is natural that the active sites which form effective three-phase interface in the electrocatalyst are proportional to the Pd loadings. The higher EASA means the higher three-phase interface which results in a higher catalytic activity. The highest EASA and activity were found on the electrocatalyst of 50 wt% Pd–WC/C. It also evidences the synergistic effect between Pd and WC since not only the activity of Pd–WC/C is higher but also the onset potential and peak potential are more negative compared to Pd/C even at lower Pd percentages. Similar synergistic effect has been observed on Pt–WC/C electrocatalysts for oxygen reduction reaction (ORR) [26,27]. The curves in Fig. 4 decline when the Pd contents excess 50 wt% in the electrocatalysts. The reason of the decrease in the catalytic activity at higher Pd contents is probably the weakened interaction between Pd and WC due to the reduction in the interface between Pd and WC, leading to the reduction in the synergistic effect.

The effect of temperature on the electrode activity was also tested. We firstly figured the Tafel plots of current densities against the overpotentials at different temperatures. The exchange current densities j^0 at different temperatures were obtained by extrapolating the linear Tafel lines to the point at where the overpotential equals zero. Table 2 summarizes the exchange current densities of ethanol oxidation on Pd/C and Pd–WC/C at different temperatures. The exchange current densities for ethanol oxidation on Pd–WC/C electrodes are almost two orders higher than that on Pd/C electrodes. The activity increases with the increase in the temperature. However, the effect of the temperature on the electrode activity is generally unobvious. The plots of the $\log j^0$ against the T^{-1} are shown in Fig. 5. From the following equation (Arrhenius formula) we can calculate the activation free energy:

$$\log j^0 = \log K - \frac{\Delta G^{0\neq}}{2.3RT} \quad (1)$$

or

$$\Delta G^{0\neq} = -2.3R\left[\frac{\partial \log\ j^0}{\partial(T^{-1})}\right] \quad (2)$$

where $\Delta G^{0\neq}$ is the reaction activation free energy; R the gas constant; T the temperature; K is a factor depending on the concentration.

The lower $\Delta G^{0\neq}$ means a higher activity. The values of the $\Delta G^{0\neq}$ can be obtained from the slopes of the linear relationship between $\log j^0$ and T^{-1} from Fig. 5. The lower $\Delta G^{0\neq}$ for the ethanol oxidation on Pd–WC/C of 10.59 J mol^{-1} was obtained against 26.96 J mol^{-1} on Pd/C. The results are consistent with the electrochemical results. This is also a possible reason for the significant improvement of ethanol oxidation on Pd–WC/C electrocatalyst in alkaline media.

Table 2
Exchange current densities of ethanol oxidation on Pd/C and Pd–WC/C at different temperatures

Temperature (K)	Pd/C, j^0 (A cm^{-2})	Pd–WC/C, j^0 (A cm^{-2})
303	6.40×10^{-6}	1.45×10^{-4}
313	6.71×10^{-6}	1.46×10^{-4}
323	7.03×10^{-6}	1.48×10^{-4}
343	7.32×10^{-6}	1.53×10^{-4}
363	7.89×10^{-6}	1.55×10^{-4}

4. Conclusion

Tungsten carbide single nanocrystal was prepared by the optimized intermittent microwave heating (IMH) technique. TEM, fast Fourier transform (FFT) of the HRTFM and XRD measurements showed that the as-prepared tungsten carbide is a hexagonal WC single crystal and is grown along zone axis [0 0 1] with the lattice spacings of $d = 2.556$ Å and $d = 2.586$ Å. The average WC particle size is about 20 nm. Pd supported on tungsten carbide electrocatalysts (Pd–WC/C) were prepared and used for the oxidation of ethanol in alkaline media. The Pd–WC/C electrocatalyst showed a tremendously high activity compared to that of Pd/C with the more negative onset potential and higher peak current densities. The activation free energy for the reaction on Pd–WC/C electrocatalyst is significantly reduced. A volcano

relationship between the ratios of the EASAs or the ratios of peak current densities and the percentage of Pd in the electrocatalysts was found. The synergistic effect which responses the high activity was evidenced.

Acknowledgement

The authors gratefully acknowledge the support by the NNSFC (20476108).

References

[1] S. Ye, A. Vijh, L. Dao, J. Electroanal. Chem. 415 (1996) 115.
[2] L. Zhang, J. Zhang, D.P. Wilkinson, H.J. Wang, J. Power Sources 156 (2005) 171.
[3] R.W. Reeve, P.A. Christensen, A.J. Dickinson, A. Hamnett, K. Scott, Electrochim. Acta 145 (2000) 3463.
[4] N. Alonso-Vante, H. Tributsch, Nature 323 (1986) 431.
[5] N. Alonso-Vante, W. Jaegermann, H. Tributsch, W. Honle, K. Yvon, J. Am. Chem. Soc. 109 (1987) 3251.
[6] M. Boudart, R.B. Levy, Science 181 (1973) 547.
[7] S.T. Oyama, J.C. Schlatter, J.E. Metcalfe, J.M. Lambert, Ind. Eng. Chem. Res. 27 (1988) 1639.
[8] R. Venkataraman, H.R. Kunz, J.M. Fenton, J. Electrochem. Soc. 150 (2003) A278.
[9] X.G. Yang, C.Y. Wang, Appl. Phys. Lett. 86 (2005) 224104.
[10] H. Chhina, S. Campbell, O. Kesler, J. Power Sources 164 (2007) 431.
[11] G. Vèrtes, G. Horányi, S. Szakács, J. Chem. Soc., Perkin Trans. II (1973) 1400.
[12] G. Horányi, G. Vèrtes, J. Chem. Soc., Perkin Trans. II (1975) 827.
[13] B. Harald, Nature 227 (1970) 483.
[14] H.H. Hwu, J.G. Chen, J. Phys. Chem. B 105 (2001) 10037.
[15] J. Lemaiter, B. Vidick, B. Delmon, J. Catal. 99 (1986) 415.
[16] J.A. Nelson, M.J. Wagner, Chem. Mater. 14 (2002) 1639.
[17] H.X. Zhong, H.M. Zhang, Y.M. Liang, J.L. Zhang, M. Wang, X.L. Wang, J. Power Sources 164 (2007) 572.
[18] F.H. Ribeiro, R.A. Dalla Betta, G.Y. Guskey, M. Boudart, Chem. Mater. 3 (1991) 805.
[19] G.L. Tan, C.H. Chen, S.C. Cheang, K.M. Uang, Appl. Phys. Lett. 85 (2004) 2358.
[20] H.J. Zheng, C.A. Ma, W. Wang, J.G. Huang, Electrochim. Commun. 8 (2006) 977.
[21] S.V. Pol, V.G. Pol, A. Gedanken, Adv. Mater. 18 (2006) 2023.
[22] G.H. Li, C.A. Ma, J.Y. Tang, J.F. Sheng, Electrochim. Acta 52 (2007) 2018.
[23] R. Ganesan, J.S. Lee, Angew. Chem. Int. Ed. 44 (2005) 6557.
[24] G.H. Li, C.A. Ma, J.Y. Tang, Y.F. Zheng, Mater. Lett. 61 (2007) 991.
[25] G.H. Li, C.A. Ma, Y.F. Zheng, W.M. Zhang, Micropor. Mesopor. Mater. 85 (2005) 234.
[26] H. Meng, P.K. Shen, Chem. Commun. (2005) 4408.
[27] H. Meng, P.K. Shen, J. Phys. Chem. B 109 (2005) 22705.
[28] M. Nie, P.K. Shen, Z.D. Wei, J. Power Sources 167 (2007) 69.
[29] F.P. Hu, F.W. Ding, S.Q. Song, P.K. Shen, J. Power Sources 163 (2006) 415.
[30] P.K. Shen, C.W. Xu, Electrochim. Commun. 8 (2006) 184.
[31] Z.Y. Wang, F.P. Hu, P.K. Shen, Electrochim. Commun. 8 (2006) 1764.